The ground and ionized states of azulene; a combined study of the vibrational energy levels by photoionization, configuration interaction and density functional calculations.

Michael H. Palmer,[1,a] Marcello Coreno,[2,b] Monica de Simone,[3,b] Cesare Grazioli,[3,b] Nykola C. Jones,[4,b] Søren Vrønning Hoffmann[4,b] and R. Alan Aitken[5,b]

[1] *School of Chemistry, University of Edinburgh, Joseph Black Building, David Brewster Road, Edinburgh EH9 3FJ, Scotland, UK.*

[2] *ISM-CNR, Instituto di Struttura della Materia, LD2 Unit 34149 Trieste, Italy.*

[3] *IOM-CNR, Istituto Officina dei Materiali, Basovizza SS-14, Km 163.5, 34149 Trieste, Italy.*

[4] *ISA, Department of Physics and Astronomy, Aarhus University, Ny Munkegade 120, DK-8000, Aarhus C, Denmark.*

[5] *School of Chemistry, University of St Andrews, North Haugh, St Andrews, Fife, KY16 9ST, Scotland, UK.*

[a] Email: *m.h.palmer@ed.ac.uk*:

[b] Electronic addresses: *marcello.coreno@elettra.eu; desimone@iom.cnr.it; grazioli@iom.cnr.it; nykj@phys.au.dk; vronning@phys.au.dk; raa@st-andrews.ac.uk*

ABSTRACT

A synchrotron-based photoionization spectrum of azulene shows significant additional vibrational fine structure when compared to previous studies. This spectrum was successfully analysed by Franck-Condon (FC) methods. Previously reported zero-kinetic-energy electron spectra (ZEKE) for azulene, have been reinterpreted in FC terms, leading to some alternative assignments to the earlier work. The sequence of ionic states has been determined by *ab initio* configuration interaction (CI) methods, leading to reliable theoretical values for both the calculated adiabatic and vertical ionization energies (AIE and VIE respectively). VIE were calculated by both symmetry-adapted cluster (SAC-CI), together with Green's function (GF) and Tamm Dancoff approximation (TDA), single excitation CI methods; AIE for highest states of each symmetry, were determined by open-shell self-consistent field (SCF) methods at the restricted Hartree-Fock level. Complete active space SCF(CASSCF) was used for the pairs of states $1^2A_2 + 2^2A_2$ and $1^2B_1 + 2^2B_1$ each of which occurs as antisymmetric and

symmetric (higher energy) combinations. The combined ionic state sequences (AIE and VIE) from these methods are $1^2A_2 < 1^2B_1 < 2^2A_2 < 2^2B_1$. The PES shows a series of broad bands above 11 eV, each of which are attributed to more than one ionisation. The calculated PES sequence of states up to 19 eV shows the SAC-CI and GF results are in almost exact agreement. The internal spacing of the bands is best reproduced by the simpler GF and TDA methods. States involving simultaneous ionization and electronic excitation are considered by both SAC-CI and TDA methods.

I.   INTRODUCTION

Recently, we reported synchrotron based, high-resolution photoelectron spectra (PES) and vacuum ultraviolet (VUV) absorption spectra for some highly conjugated molecules, including cyclooctatetraene (COT),[1,2] cycloheptatriene (CHT) [3,4] and norbornadiene (NBD).[5,6] Through-space interactions between non-bonded degenerate C=C π-bonds occur in these molecules.

We now report a new PES study of the fully conjugated molecule azulene (*1*) which is isomeric with naphthalene (*2*); both are shown in Figure 1.[7-10] We demonstrate significantly higher spectral resolution than previously reported for *1*.[11-13] The additional vibrational structure disclosed is analysed by Franck-Condon methods. Although both *1* and *2* are fully conjugated, azulene has some properties more like those of a deca-1,3,5,7-pentaene, where the C_9C_{10} bond is replaced by two H-atoms. The contrasts between *1* and *2* include colour, where *1* is azure blue in colour (hence the name), while *2* and most other hydrocarbons are colourless.

Microwave spectral (MW) studies of the ground X^1A_1 state of azulene show a planar structure with C_{2v} symmetry.[14,15] Gaseous *1* has a significant dipole moment (Figure 1, DM),[14,15] in contrast to *2* which is nonpolar. The most accurate value for the azulene DM, shown in Figure 1, is μ_A 0.8821 ± 0.0024 Debye, measured by microwave spectroscopy (MW);[9] values in solution are significantly higher. The azulene DM involves electron charge transfer from the 7- to the 5-membered ring; the configuration in Figure 1, shows full transfer of 1-electron ($\delta = 1$), whereby each ring effectively contains 6π-electrons, through sharing of those attributed to the C_9C_{10}-bond.[9]

These two compounds are classic alternant (**2**, AH) and non-alternant hydrocarbons (**1**, NAH). In the AH series, the C-atoms can be marked by stars, such that no two starred atoms are adjacent; this cannot be avoided in NAH systems owing to the odd-membered (5,7) rings.
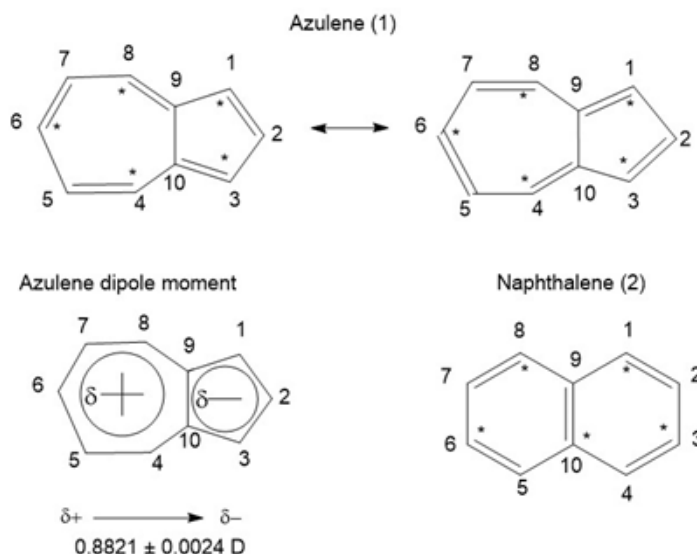
Figure 1. Structures of azulene (1) and naphthalene (2)

Eland and Danby (E&D),[11] performed the earliest PES and electron impact (EI) studies on azulene; the energetic results differ by up to 0.3 eV. The E&D PES gave a series of broad peaks, with vertical IE reported as: 7.42, 8.49, 9.91, 10.81eV; other than VIE_3, these are effectively identical to Boschi et al,[12] who give VIE_3 10.07 eV. In both these studies,[11,12] IE_4 close to 11 eV is not a true maximum. In contrast, we observe a sharp peak at 10.9 eV, followed by further poorly defined maxima up to 11.6 eV.

Weber et al[13] generated a PES spectrum from azulene by resonant two-photon excitation at 293.17 and 282.3 nm; these wavelengths generate the 3rd and 4th singlet excited states (S_3 and S_4) respectively. The most significant feature of these spectra is that the azulene cations are generated with a very large amount of vibrational energy, leading to largely featureless bands;[13] these are not directly comparable to conventional PES.

The new PES vibrational results also allow us to reconsider assignments of earlier mass-selected ion-current spectra and zero-kinetic-energy (ZEKE) electron spectra by Tanaka et al.[16] These were performed for *both* azulene *and* its van der Waals complex with argon in a supersonic jet.[17] This also

used two-photon $(1+1^/)$ resonant ionization via S_2. The AIE for these two species are 59781(5) cm^{-1} (7.4118 eV, **1**) and 59708(5) cm^{-1} (7.4027 eV, **1+Ar**) respectively,[16] showing a difference of only 73 cm^{-1}. The free azulene ZEKE spectrum showed a 0-0 band at the S_2 origin, accompanied by several vibrational bands with frequencies: 239, 373, 468, 661, 746, 886 and 918 cm^{-1}. The observed fundamental frequencies in the fluorescence spectra excited at the 236 and 468 cm^{-1} bands correspond to the ν_{39} (326 cm^{-1}) and ν_{38} (477 cm^{-1}) modes respectively, both of b_1 symmetry. Similarly, the ν_{16} (a_1, 662) and ν_{37} (b_1, 668 cm^{-1}) bands in the absorption spectrum were thought to be active. Thus, in those studies, non-symmetric vibrations were proposed for some observed vibrations, based on fluorescence spectra obtained by Fujii et al,[17] from the S_2, S_3 and S_4 excited states to the ground state (S_0) of azulene. Modes 37, 38 and 39, vibrations of b_1 symmetry, were thought to arise from vibronic coupling. We will offer an alternative assignment involving fully symmetric bands below. In both these ZEKE and fluorescence studies, the labels b_1 and b_2 for vibrational modes are interchanged relative to the present study;[18] both conventions lead to identical numerical results and are a result of different coordinate systems being used for the molecule.

This paper discusses the ionic states of azulene determined by both PES and ZEKE; similar discussion of the ground and corresponding singlet and triplet state manifolds is deferred to a later paper. Our experimental results are interpreted by high-level theoretical studies, including symmetry adapted cluster (SAC-CI), complete active space SCF (CASSCF) and CI calculations. We perform Franck-Condon vibrational state analyses of our new synchrotron-based PES, using the Pisa group software[19-21] incorporated in Gaussian-16 (G-16),[22] where processing of the vibrational analysis is limited to a single imaginary frequency. Some highly bound ionic states generate imaginary frequencies, implying that the structures are saddle points rather than genuine minima.

II. METHODS

The azulene sample, CAS registry number 275-51-4, purchased from Sigma-Aldrich (product number A97203, 99% purity), was used without further purification.

A. The UV-photoelectron spectrum of azulene.

This was obtained at room temperature on the gas-phase line of the Elettra synchrotron (Basovizza, near Trieste, Italy), using methods described previously.[1,3] The azulene vapour was irradiated with both 30 eV and 40 eV photon energies. The 30 eV spectrum covers the energy range 7.057 to 14.257 eV with 4571 data points (DPs), separated by 0.001 eV (8 cm^{-1}) up to 9.357 eV, with 0.002 eV separation at higher energy. A wider scan up to 19.180 eV, using 40 eV irradiation, contained 1251 DPs, with a separation of 0.01 eV.

The 30 eV spectrum corresponds to an overall resolution close to 8.5 meV; we adopt a conventional definition of resolution as the minimum separation between two lines where it is possible to distinguish between them. The precision of the measured energies and the resolution were also determined from argon PES lines which are known from the literature. Ar is added to the sample as an additional calibrant.

The absolute positions of the principal PES bands, determined by the program Multi-peak Fit (Version 2.22), are shown in Figure 2 and Table I; additional peak-fit statistics are shown in the supplementary material as SM1.The peak separations shown in Table I are relevant to the Franck-Condon separations determined theoretically below. Previous vibrational separations reported by Boschi et al [12] for the lowest ionization of azulene are: 830, 1130, 1340 and 1990 cm^{-1}, where all are ± 70 cm^{-1}; the values in Table 1 are consistent with these earlier results, although ours have a smaller uncertainty.

Table I. Peak positions from the multi-peak analysis; errors in the last digit shown are in parentheses.

Band A				Band B			
Peak label	Location /cm^{-1}	Location /cm^{-1}	Peak separation/ cm^{-1}	Peak label	Location / cm^{-1}	Location / cm^{-1}	Peak separation/ cm^{-1}
P0	7.305(2)	58920	0	P10	8.47(5)	68316	-165
P1	7.409(1)	59758	838	P11	8.490(1)	68481	0
P2	7.455(1)	60130	1210	P12	8.534(1)	68833	352
P3	7.512(1)	60590	1670	P13	8.603(1)	69388	907
P4	7.560(1)	60975	2055	P14	8.688(1)	70073	1592
P5	7.536(5)	60981	2061	P15	8.70(1)	70204	1723
P6	7.578 (5)	61126	2206				
P7	7.665(1)	61823	2903				
P8	7.77(2)	62670	3750				
P9	7.715(1)	62225	3305				

Figure 2. Location of peak maxima for Bands A and B. There is evidence of a hot-band at the onset to Band B. Peaks 1 to 15 (red) are individual fits to peaks observed, as listed in Table I; residuals are shown in green above. These represent a very small proportion of the overall PES counts shown. The red peaks shown indicate position only, and their intensities are scaled to fit, leaving the residuals shown.
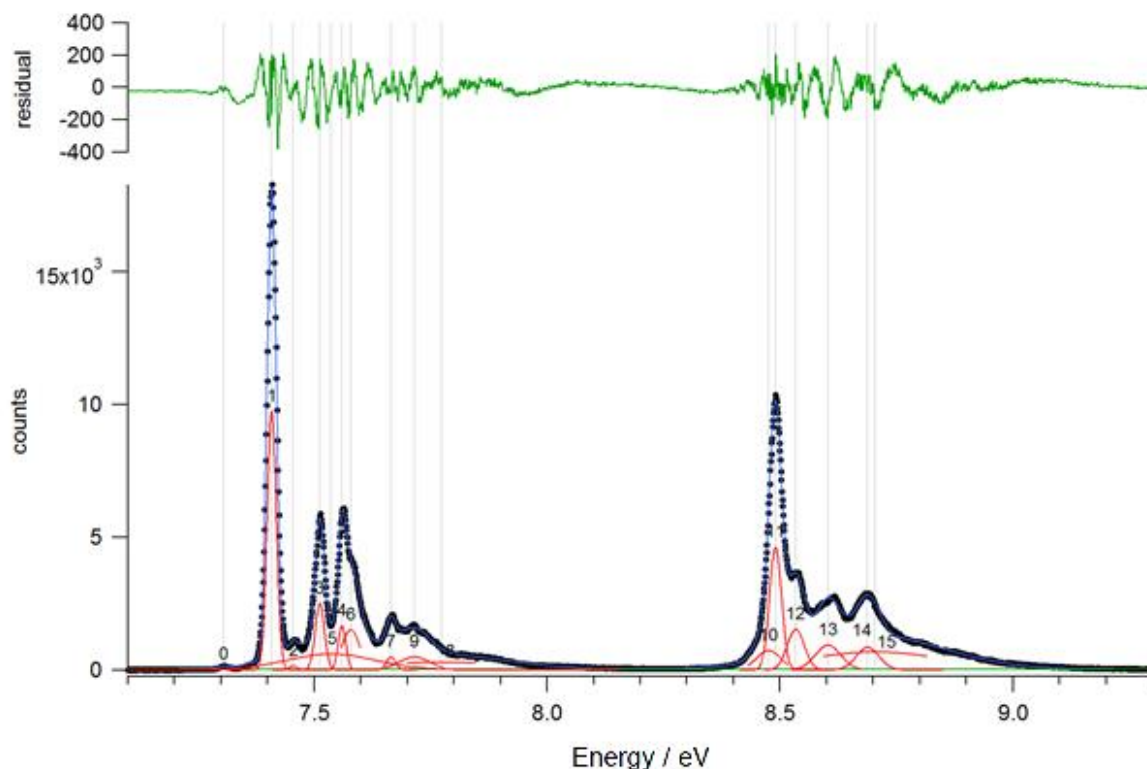
B.   Theoretical methods.

Several computational chemistry suites were used since none offers us a complete analysis. The equilibrium structures for the X^1A_1 ground state and several of the lowest ionic states of each symmetry were determined by (restricted) open shell Hartree-Fock (RHF) calculations using the G-16 suite.[22] Several density functional theory (DFT) functionals[23] were tested, including the Becke + (3-parameter) Lee–Yang–Parr (B3LYP) hybrid functional.[24] Overall, a long-range-corrected version of B3LYP, the Coulomb-attenuating method (CAM-B3LYP),[25] proved to give the best results; this was in terms of energy separations between ionic states, and also in terms of balance between the 0-0 band and vibrational satellite intensities determined by the Pisa software discussed below. A double

6

hybrid method, B2PLYPD3, combining a Møller-Plesset type of correlation within a DFT calculation, gave good adiabatic ionization energies (AIE),[26-28] but a very high proportion of the intensity was concentrated in the 0-0 band and a very much lower intensity for the fundamentals and combination bands. This contrasts with the PES spectral profile.

The RHF-method incorporating the CAM-B3LYP procedure was only applicable to the lowest ionic state of each symmetry. To determine the AIE for higher members of these manifolds, complete active space self-consistent field (CASSCF) calculations were performed for the pairs of states $1^2A_2 + 2^2A_2$ and $1^2B_1 + 2^2B_1$ states, using G-16.[22] These calculations included 7-electrons permuted into 8-MOs, conventionally termed CASSCF [7,8], and generated 3920 configurations. The higher energy states, 2^2A_2 and 2^2B_1 states, proceeded normally using this method,[22] by choice of the 2nd root for optimization in 2-root searches. These CASSCF calculations generated linear combinations of states such as $1^2A_2 \pm 2^2A_2$. All these RHF and CASSCF calculations gave wave-functions which were input to the Pisa software as described below.

Although a more general solution to this problem would be the use of the MCSCF package in the MOLPRO suite,[29] where both the root and the symmetry are selected, this package does not produce output which is currently acceptable to our version of the Pisa software. Some MOLPRO results for structures of higher roots are shown in the supplementary material as SM2.

C.   Basis sets.

Modern bases deliberately contain a wide range of exponents, which cater for both valence and Rydberg state determination. Ionic states strongly require valence shell functions. Such Gaussian-type orbitals (GTOs) are present in various older basis sets such as 6-311G(d,p),[30,31] otherwise known as 6-311G,** which is used in the main thrust of this work.

III. RESULTS

A. Structures.

Microwave spectroscopy shows that the molecular structure of azulene is a relatively rigid molecule[14,18] with rotational constants (RC) A = 2841.951(24), B = 1254.84634(10) and C =

870.7162(8) MHz.[14] The RC for the equilibrium structure of azulene using the 6-311G(d,p) basis set in the RHF method, are very similar with: A = 2876.87, B = 1265.89 and C = 879.08 MHz. This basis is also used for all the ionic state structures undergoing analysis, namely the 1^2A_2, 1^2B_1, 2^2A_2, 2^2B_1 and 1^2A_1 states. Since equilibrium structures are not the focus of this paper, they are shown in the supplementary material as SM3. The vibrational structure for each of these states is discussed below.

B.   Assignment of the wide scan azulene photoelectron spectrum from 6.5 to 19 eV.

The wide PES scan measured with 40 eV photon irradiation is shown in Figure 3, with bands designated as A to M for simplicity, although some such as D+E, F+G and H+I contain overlapping members. Only 3 bands A, B and D show well-defined vibrational structure, as discussed below. In the following Sections we present new assignments for (a) the vertical ionization energies (VIE) of numerous valence shell ionic states, together with their relative intensities; (b) adiabatic excitation energies (AIE) together with their vibrational structure, which will be analysed by Franck-Condon methods.
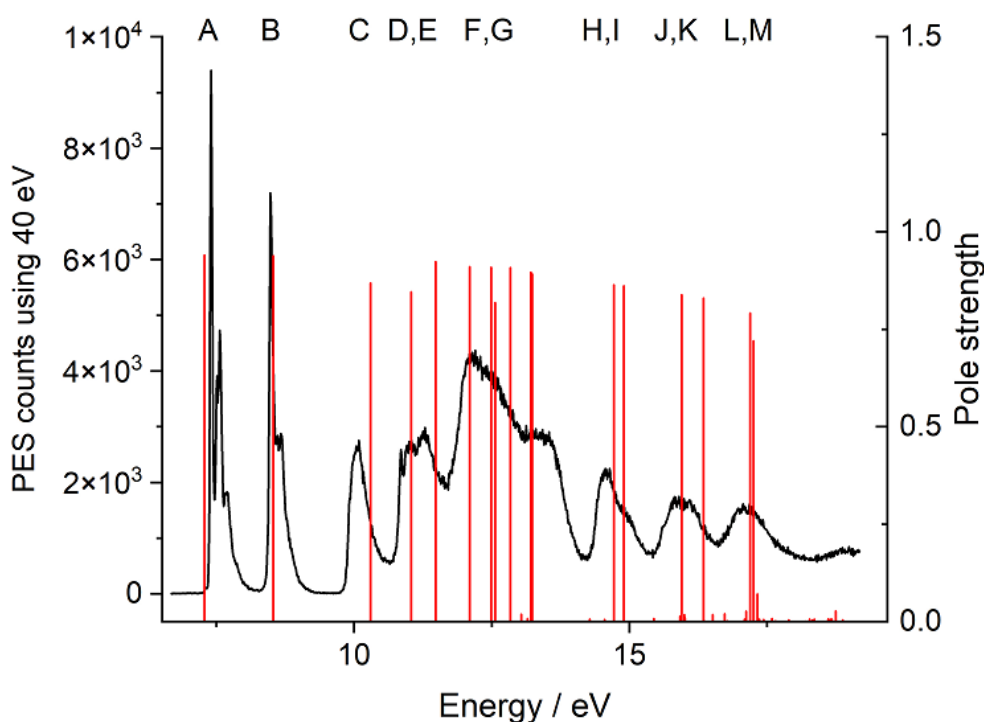
Figure 3. The wide scan photoelectron spectrum (PES) of azulene using 40 eV irradiation (black curve), with the SAC-CI monopole strengths (red lines). The principal bands of the PES have been labelled A to M for ease of description in the text. The energies (eV) have been scaled using the equation $VIE_{pes} = 0.90*VIE_{calc} + 1.30$. A set of well-defined IE were chosen. The energies of the calculated peaks closest to these ionizations, were then plotted against the measured set,

establishing a correlation line. All the calculated energies were then scaled by that correlation equation. The same applies for Figure 4.

The most intense PES bands are often denoted as Koopmans' theorem bands (KT); these are where almost all the intensity of the band is represented by a 1-electron (1e) process; for example, the highest occupied molecular orbital ($2a_2^2$) has a single electron removed, generating $2a_2^{-1}$; in KT processes involving this MO, this configuration is dominant, and the energy of the KT state is close to the occupied orbital energy for that configuration. Structural relaxation in the ion is variable, but can be substantial, with consequential lowering of the energy. Many weaker bands are also present, where ionization is accompanied by electronic excitation; these are 2-electron (2e) processes, widely known as shake-up states. We present theoretical results for both 1e- and 2e-states, including ionic state energies (eV) and their intensities (pole strengths).

We assign the overall PES envelope over the range shown in Figure 3, utilising several methods; (a) our most rigorous level, used the symmetry-adapted coupled cluster method developed by Nakatsuji et al (SAC-CI),[32-36] as installed in G-16.[22] (b) In contrast, the Green's function (GF) method for 1e processes only, and Tamm-Dancoff approximation (TDA), which includes 2e-processes, both single excitation CI[37-39] methods, are implemented in GAMESS-UK.[40]

The theoretical manifold shown in Figure 3, uses the SAC-CI model. Above 12 eV several very weak lines are apparent, which are 2e-processes. In general, the SAC-CI method gives a good account of the PES profile, but with the onset peaks and those near17 eV being used for the range of the PES fit, the peaks near the centre of the PES, from 10 to 13 eV, especially for IE_3 and IE_{4+5} do not give close fits. The active MOs used in the SAC-CI calculations are full valence shell range.

The TDA results in Figure 4 give a much closer fit for $IE_{3,4,5}$; this also shows the 2e-processes more dramatically; their simplicity in calculation and interpretation makes these the choice in the current study. The high energy range close to 20 eV is uneven in the TDA theoretical intensities; this arises from the physical limits imposed on the range of active MOs (20 for each representation) in the TDA code. Thus, some excitations which are necessary for a smooth curve are excluded. GF is presented

9

in the supplementary material as SM4; its results are similar to both the SAC-CI and TDA, but the decline in pole strengths with energies seems delayed relative to the PES experiment.

Deleuze et al[41] reported theoretical PES of azulene using a third-order algebraic diagrammatic construction (ADC (3)) scheme similar to TDA. They suggested that two 2e-processes occur after the 2nd ionization band (B), with energies close to 9.6 and 10.6 eV. The present onset for 2e-processes using the TDA method are higher energy at 10.08 and 11.20 eV. The Deleuze et al[41] calculations used both a low resolution PES, and theoretical line widths, denoted by Full Width at Half Maximum (FWHM) of *0.5 to 1.0 eV*. In our fits below, we use FWHM down to 10 cm^{-1}, and hence show much more detail, and also with a more balanced aspect ratio.
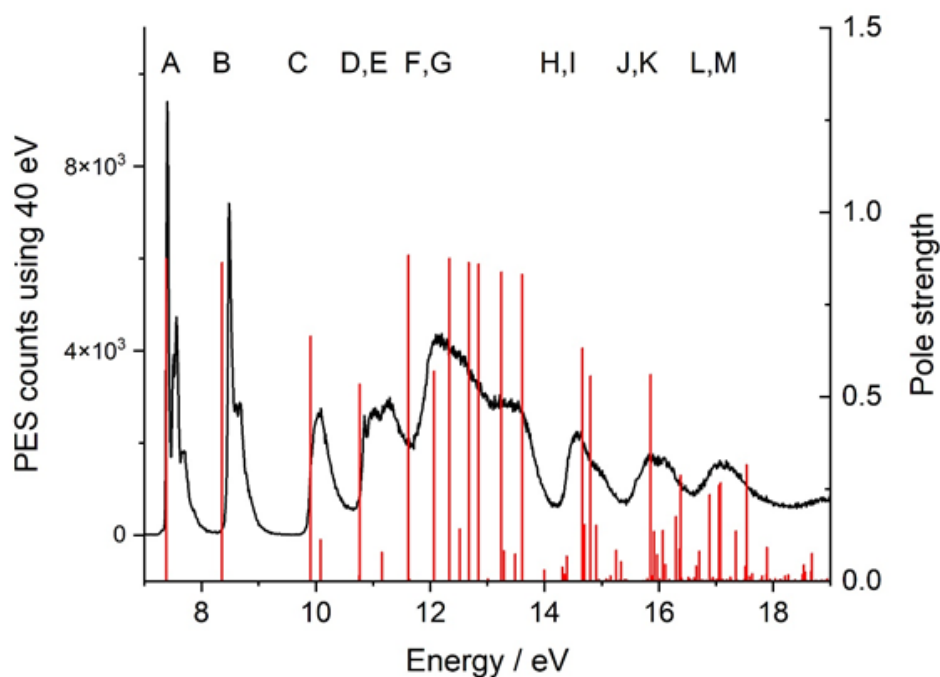
Figure 4. The wide scan photoelectron spectrum (PES) of azulene using 40 eV irradiation (black curve), with the TDA monopole strengths (red lines). The principal bands of the PES have been labelled A to M for ease of description in the text. The energies (eV) have been scaled to fit the spectral range using the equation $VIE_{pes} = 0.875*VIE_{calc} + 1.368$.

The principal numerical 1e-results of the open-shell CI calculations by SAC-CI and Green's function methods are shown in Table II. The SAC-CI VIE are lower by 0.248 eV on average; this makes VIE_3 and VIE_4 difficult to correlate with experiment. The first change of VIE between the methods occurs above 18 eV, with $10a_1$ and $7b_2$, the same position where the 1e-processes collapse with the onset of

a dense 2e-profile. The results depicted in Table II show a considerable similarity in the VIE using either SAC-CI or GF methods over 17 valence MOs, with a linear correlation: $VIE_{GF} = 0.996(8)$ $*VIE_{SACCI} + 0.248(110)$. The correlation coefficient (adjacent R^2) is 0.9989 and standard errors are in parentheses. The two sets of results are effectively identical for 1e-processes; this level of agreement is unexpected and very satisfactory. The GF and TDA single excitation CI method calculations are dramatically shorter in processor time than the SAC-CI, a coupled cluster procedure. The computational cost of SAC-CI is larger by an order of magnitude, and this is likely to be its main limitation at present.

Table II. The vertical ionization energies for azulene. (a) Symmetry adapted cluster configuration interaction (SAC-CI); (b) determined by Greens' function 3rd order perturbation theory. All electron numbering is used to assist comparison with earlier studies. These are the theoretical results, which have been scaled to fit in the correlation with the experimental PES discussed below. The first difference in the ionic state sequences occurs with $10a_1$ and $7b_2$ at 17.851 and 20.538 eV respectively.

Orbital vacated	SAC-CI		Green's function		State
	Energy / eV	Monopole strength	Energy / eV	Monopole strength	
$2a_2$	6.646	0.940	7.040	0.888	**1^2A_2**
$3b_1$	7.921	0.938	8.165	0.887	**1^2B_1**
$1a_2$	9.996	0.869	10.133	0.827	**2^2A_2**
$2b_1$	10.789	0.846	11.008	0.780	**2^2B_1**
$17a_1$	11.316	0.923	11.428	0.895	1^2A_1
$12b_2$	12.076	0.910	12.164	0.886	1^2B_2
$1b_1$	12.522	0.818	12.765	0.780	**3^2B_1**
$11b_2$	12.527	0.908	12.871	0.885	2^2B_2
$16a_1$	12.619	0.908	12.643	0.885	2^2A_1
$15a_1$	13.167	0.892	13.304	0.871	3^2A_1
$10b_2$	13.419	0.896	13.643	0.870	3^2B_2
$9b_2$	14.861	0.863	15.025	0.856	4^2B_2
$14a_1$	14.974	0.861	15.159	0.844	4^2A_1
$13a_1$	16.117	0.838	16.354	0.835	5^2A_1
$8b_2$	16.605	0.830	16.699	0.801	5^2B_2
$12a_1$	17.529	0.791	17.762	0.790	6^2A_1
$11a_1$	17.714	0.720	18.070	0.674	7^2A_1

For all VIE below 17 eV, the calculated 1e-pole strengths are generally in the range 0.7 to 0.9, and close to the limiting value of 1.0; at higher energy a rapid drop to zero occurs. Up to this limit, it is reasonable to use MO electron 1e-vacancies interchangeably with 1e-states, even though considerable electron reorganisation between the neutral and ionic states will have occurred; thus

$2a_2^{-1}$ is a good representation of 1^2A_2. This correlation between orbitals and states breaks down when 'shake-up' states occur.

Within states of the same symmetry, there is a trend for the pole strength to decline with an increase in binding energy. This is particularly striking with the $1b_1$ and $2b_1$ states, which have lower values than $3b_1$; a similar change occurs for $2a_2$ over $1a_2$.

The lowest calculated ionic state energies have the sequence: $1^2A_2 < 1^2B_1 < 2^2A_2 < 2^2B_1 < 1^2A_1 < 1^2B_2$, with SAC-CI, GF and TDA methods. Boschi et al[12] give the same sequence for the lowest four IE, but their energy values are significantly different from ours. Their onset for the σ-IE sequence starts at 11.0 eV; this would be associated with our 3^2B_1 ionization. Early *ab initio* calculations on naphthalene and azulene by Buenker and Peyerimhoff[42] drew attention to the intermingling of $\pi-$ and $\sigma-$levels in their occupied orbitals, with ascending sequences of energy, based on orbital energies, with azulene: $\pi,\pi,\pi,\pi,\sigma,\sigma,\pi$ and naphthalene: $\pi,\pi,\pi,\pi,\sigma,\sigma,\sigma,\pi$.

C.   Vibrational structure shown in the PES bands.

The following sections represent the first detailed analysis of the vibrational structure of the azulene PES. All orbitals and electrons are included in our computations; but we use valence shell numbering for occupied and virtual molecular orbitals (MOs and VMOs), to facilitate comparison with other work.

In the Franck-Condon results shown in the Tables, the molar absorption coefficient intensities are: $dm^3.mol^{-1}.cm^{-1}$. The 48 fundamental modes of azulene in C_{2v} symmetry are: $17a_1 + 6a_2 + 9b_1 + 16b_2$. Those of a_1 and b_2 symmetry correspond to in-plane vibrations while those of a_2 and b_1 symmetry are out-of-plane deformations. In conventional infrared spectroscopy modes are sequenced $a_1 < a_2 < b_1 < b_2$; these are a_1: 1-17; a_2: 18-23; b_1: 24-32; b_2: 33 - 48. However, the Franck-Condon analyses using the Pisa suite follow the G-16 convention of labelling modes from lowest to highest frequency, irrespective of symmetry. In more conventional spectroscopic notation, the highest is $1a_1$ and goes via a_2 and b_1 to the lowest $16b_2$. For simplicity and to avoid errors, we refer to prominent fundamentals present in the calculated envelopes by calculated frequency using the Gaussian-16 labels. *It is*

important to note that the ZEKE and fluorescence studies discussed below, do not adhere to the standard sequence for vibrational frequencies by state, as above. They use 1-17; a_2: 18-23; b_1: 24-39; b_2: 40 – 48. Thus, our discussion of the ZEKE spectrum adopts their sequence to maintain backwards compatibility. Full sets of harmonic frequencies for each electronic state studied, including the X^1A_1 ground state, are shown in the supplementary material as SM5. A full list of a_1 symmetry frequencies, determined with the CAM-B3LYP method and the 6-311G(d,p) basis set is shown in Table III; these are used in the FC analyses.

Table III. The CAM-B3LYP calculated a_1 symmetry harmonic frequencies, rounded to integral cm^{-1} values, used in the Franck-Condon (FC) analyses for the ionic states of azulene. In FC states, only a_1 modes are active. In Gaussian-16, these have sequential numbering from lowest (mode 1) to highest frequency (mode 48). The Pisa Group software, internal to G-16, continues this system. This numbering differs from the standard system used in vibrational spectroscopy. The position of the a_1 modes in the overall C_{2v} sequence vary with the electronic state. The sequence numbers in parentheses ({}), are those used in the FC analyses shown in Tables IV onward.

| FC mode	State					
	X^1A_1	1^2A_2	1^2B_1	2^2A_2	2^2B_1	1^2A_1
1	415{5}	410{6}	406{6}	423{6}	414{7}	320{5}
2	692{10}	696{10}	670{10}	709{11}	687{10}	465{7}
3	845{16}	859{15}	830{16}	883{16}	882{13}	730{12}
4	924{18}	911{17}	913{18}	968{20}	918{15}	866{15}
5	978{21}	974{19}	951{19}	1011{22}	966{16}	965{18}
6	1093{26}	1114{26}	1053{22}	1167{26}	1095{23}	1087{24}
7	1257{29}	1255{28}	1264{29}	1280{28}	1334{29}	1136{26}
8	1322{30}	1275{30}	1305{30}	1315{29}	1364{30}	1256{29}
9	1447{34}	1452{34}	1431{33}	1530{34}	1519{33}	1314{30}
10	1512{36}	1515{37}	1510{35}	1612{36}	1575{35}	1502{34}
11	1611{38}	1619{38}	1589{37}	1667{37}	1637{35}	1609{36}
12	1679{40}	1635{39}	1682{39}	1731{38}	1750{39}	1679{38}
13	3155{41}	3186{41}	3183{41}	3336{40}	3341{41}	3008{40}
14	3165{43}	3195{43}	3190{43}	3343{42}	3356{43}	3183{42}
15	3193{45}	3211{45}	3215{45}	3370{44}	3372{45}	3191{43}
16	3217{46}	3241{46}	3238{46}	3383{45}	3390{46}	3223{45}
17	3244{48}	3265{48}	3266{48}	3404{47}	3408{48}	3263{46}

1. Band A: the $^2A_2$ state.

The high resolution structure of the lowest ionized state, the 1^2A_2 state, is shown in Figure 5, with the detailed vibrational bands from Table IV superimposed. The most detailed previous interpretation[12] for this state, was in terms of 4 vibrations, as 830, 1130, 1340 and 1990 cm^{-1}, but with a significant

degree of uncertainty ($\pm$ 70 cm^{-1}).[12] The two lowest values are relatively close to the present calculated ones for modes 15 and 26 (859 and 1114 cm^{-1}), but our strongest contributor, mode 30, is rather different at 1275 cm^{-1}. We have no fundamental close to 1990 cm^{-1}, but a series of peaks occur, starting near 61750 cm^{-1} and shown in Figure 5, could have led to this interpretation. The same overtones and binary combination bands, shown in Table IV, 1718 cm^{-1} (15^2), 2115 cm^{-1} ($28^1;15^1$) and 2134 cm^{-1} ($30^1;15^1$) etc. have frequencies in this region. Modes 6, 10, 15, 19, 26, 28, 30 and 34 all occur in the description of the 1^2A_2 state.

Table IV. Calculated energy levels, using CAM-B3LYP method, and intensities for the 1^2A_2 ionic state of azulene. All active fundamentals, other overtones; combination bands shown are based on highest intensity. Calculated energy of the 0-0 (0^0) transition: 57610 cm^{-1} (7.1425 eV).

Energy / cm^{-1}	Excitation	Intensity	Energy / cm^{-1}	Excitation	Intensity
0	0^0	632900	1619	38^1	21990
316	1^2	151	1635	39^1	23330
318	2^2	433	1666	$28^1;6^1$	4784
410	6^1	28790	1685	$30^1;6^1$	4668
607	3^2	240	1718	15^2	17610
696	10^1	53630	1770	$17^1;15^1$	7167
775	5^2	825	1811	$26^1;10^1$	1380
821	6^2	466	1863	$34^1;6^1$	3458
859	15^1	154900	1952	$28^1;10^1$	4549
879	$11^1;1^1$	1245	1971	$30^1;10^1$	7791
911	17^1	20160	2115	$28^1;15^1$	27220
974	19^1	167	2134	$30^1;15^1$	28120
1007	7^2	1779	2166	$28^1;17^1$	4536
1107	$10^1;6^1$	1659	2186	$30^1;17^1$	5339
1114	26^1	16900	2311	$34^1;15^1$	19660
1153	9^2	496	2332	$39^1;10^1$	1961
1255	28^1	77320	2363	$34^1;17^1$	4974
1269	$15^1;6^1$	6718	2370	$28^1;26^1$	2967
1275	30^1	119600	2390	$30^1;26^1$	2875
1321	$17^1;6^1$	1302	2478	$38^1;15^1$	6281
1393	10^2	2097	2511	28^2	5460
1452	34^1	92900	2530	$30^1;28^1$	19170
1515	37^1	645	2708	$34^1;28^1$	13940
1555	$15^1;10^1$	9976	2727	$34^1;30^1$	14430
1607	$17^1;10^1$	2024			
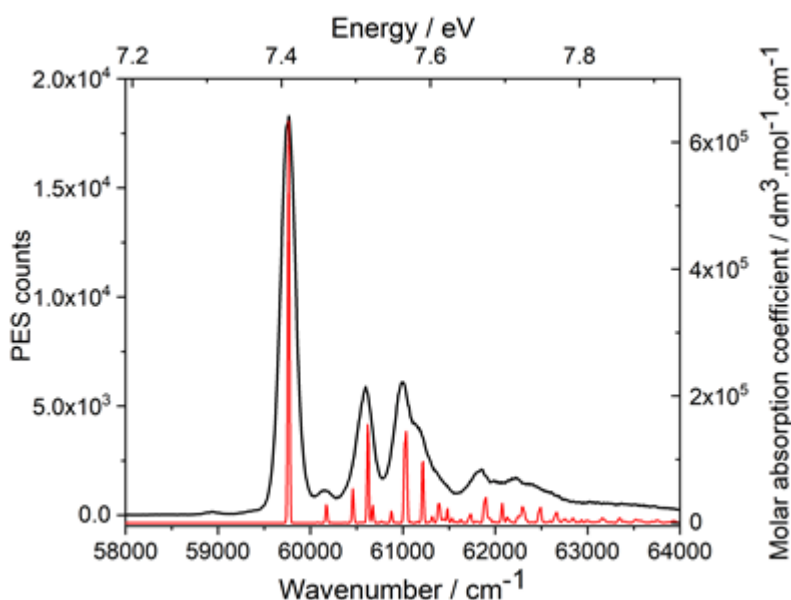
Figure 5. Azulene $^2A_2$ ionic state (black curve) with the CAM-B3LYP functional superimposed (red). The theoretical spectrum energy has been increased by 2230 cm^{-1} to overlay the experimental spectrum. The B2PLYPD3 functional gives a closer fit to the experimental AIE (energy shift only 811 cm^{-1}), but the cross-section of the theoretical spectrum is almost entirely localised (99%) in the 0-0 band.

2. Band B. The 1^2B_1 state, close to 8.5 eV.

The dominant fundamentals for band B contain major contributions from modes 6, 10, 19, 22, 29 35 and 39, especially in the combination bands shown in Table V; most of the band A fundamentals are not present in band B. Thus, the superficial similarity in structure between bands A and B, as shown in Figures 5 and 6, is accidental, the two are different in character.

Table V. Prominent theoretical Franck-Condon bands for the Band B, attributed to the 1^2B_1 state, based on CAM-B3LYP calculations.

Energy / cm^{-1}	Excitation	Intensity	Energy / cm^{-1}	Excitation	Intensity
0	0	654900	1583	$18^1;10^1$	2228
274	1^2	4548	1589	37^1	77220
406	6^1	122100	1670	$29^1;6^1$	2871
670	10^1	47900	1682	39^1	171100
811	6^2	14930	1723	$22^1;10^1$	14880
830	16^1	30250	1837	$33^1;6^1$	2882
913	18^1	35500	1883	$22^1;16^1$	10130
951	19^1	4049	1966	$22^1;18^1$	6343
955	7^2	5294	1994	$37^1;6^1$	21710
1053	22^1	136700	2088	$39^1;6^1$	28760
1076	$10^1;6^1$	12260	2105	22^2	15390
1236	$16^1;6^1$	8161	2512	$39^1;16^1$	11370
1264	29^1	17010	2641	$37^1;22^1$	19090
1319	$18^1;6^1$	5710	2734	$39^1;22^1$	31620

| 1458 | $22^1;6^1$ | 37700 | 3271 | $39^1;37^1$ | 17990 |
| 1510 | 35^1 | 14040 | 3364 | 39^2 | 22080 |
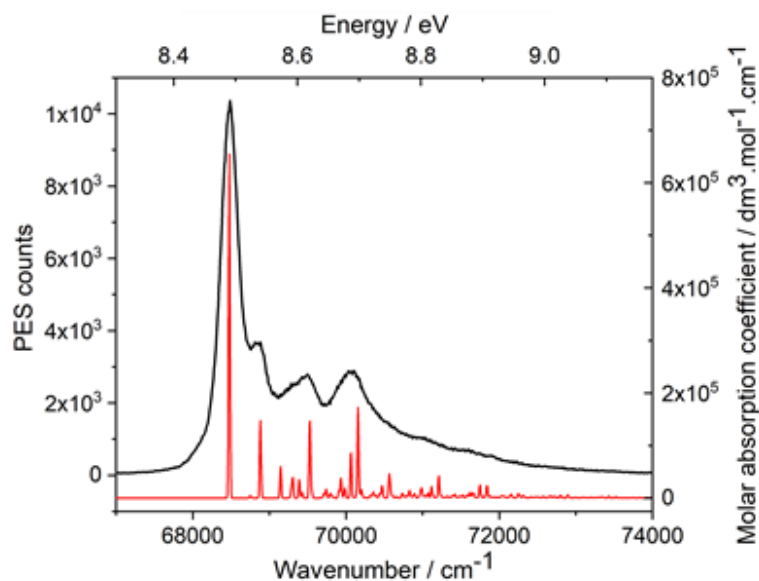
Figure 6. Azulene $^2B_1$ PES state (black curve) using the CAM-B3LYP functional, with the Franck-Condon profile superimposed (red).

### 3. Band C, the 2^2A_2 state close to 10 eV.

The analysis is dominated by modes 6, 11, 16, 22, 28, 34 and 37, but with large differences in intensity, as shown in Table VI; a short sequence in mode 6^n (n =1, 2, 3) occurs, but most of Table VI is binary combinations of these, especially with the lowest frequency mode 6. Strong ternary combination bands are more prominent in intensity than for the other ionic states. The band, shown in Figure 7, is comparatively narrow, but with a high 0-0 level.

Table VI. Band C assigned to the 2^2A_2 state, determined by CASSCF calculations: the most intense Franck-Condon bands

Energy / cm^{-1}	Excitation	Intensity	Energy / cm^{-1}	Excitation	Intensity
0	0	87870	1720	$22^1;11^1$	4906
423	6^1	63430	1729	$16^1;6^2$	9433
709	11^1	37390	1857	$22^1;6^2$	7456
846	6^2	34340	1978	$11^1;6^3$	6543
883	16^1	18360	2015	$16^1;11^1;6^1$	5848
1011	22^1	15360	2143	$22^1;11^1;6^1$	5161
1132	$11^1;6^1$	39520	2163	$28^1;16^1$	5487
1269	6^3	11920	2239	$34^1;11^1$	5404
1280	28^1	30120	2264	$11^2;6^2$	4956
1306	$16^1;6^1$	18980	2291	$28^1;22^1$	4502
1418	11^2	10490	2376	$34^1;6^2$	5130

1434	$22^1;6^1$	15440	2377	$37^1;11^1$	6054
1530	34^1	16270	2513	$37^1;6^2$	6462
1555	$11^1;6^2$	20090	2561	28^2	4576
1667	37^1	11330	2586	$28^1;16^1;6^1$	5672
1703	$28^1;6^1$	21100	2662	$34^1;11^1;6^1$	5644
1841	$11^2;6^1$	10400	2714	$28^1;22^1;6^1$	4516
1953	$34^1;6^1$	16240	2810	$34^1;28^1$	4694
1989	$28^1;11^1$	11150	2835	$28^1;11^1;6^2$	5989
2090	$37^1;6^1$	12330	2861	$16^1;11^1;6^3$	1012
2126	$28^1;6^2$	11440	3233	$34^1;28^1;6^1$	4677
2412	$28^1;11^1;6^1$	11780	3371	$37^1;28^1;6^1$	4423
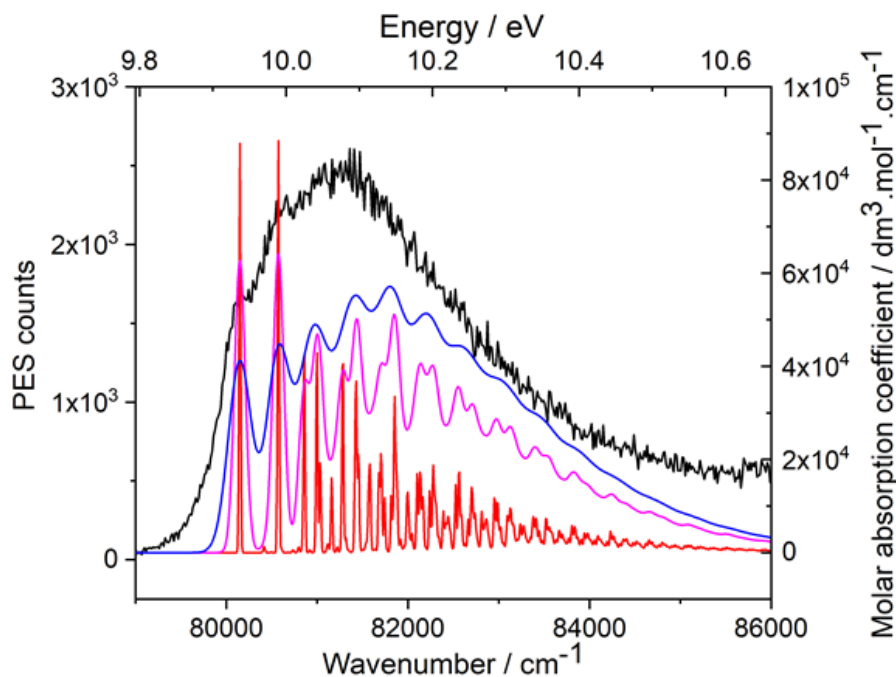
Figure 7. Azulene PES Band C (black curve) with the CASSCF 2^2A_2 state Franck-Condon envelope. The theoretical levels show sets of vibrational peaks corresponding to Half-Widths at Half-Maximum of 10 cm^{-1} (red), 70 cm^{-1} (magenta) and 150 cm^{-1} (blue).

4. Bands D and E. An overlapping set of peaks assigned to the 2^2B_1 and 1^2A_1 ionic states.

We note that a sharp peak occurs at 10.865 eV (87631 cm^{-1}) which is out of character with other nearby peaks. We assign this band D peak, to the onset of 2^2B_1 ($2b_1^{-1}$); this calculated state has a sharp 0-0 peak. In contrast, the profile for 1^2A_1, has a low onset cross-section, as shown in Table VII, and differs fundamentally from 2^2B_1.

After projection of the imaginary frequency and renumbering to account for this, the 1^2A_1 state shows the fundamentals 5, 7, 15, 18, 24, 26, 29, 34 and 36; these correspond to frequencies: 320, 465, 866, 965, 1087, 1136, 1256, 1502 and 1609 respectively. The principal components of the Franck-Condon

analysis for the 2^2B_1 ionic state is shown in Table VIII and Figure 8. The positioning of the higher component, the 1^2A_1 ionic state, shown in Table VII is uncertain, and here it is chosen to correspond to the highest part of the intensity envelope close to 11.4 eV. The positioning of the 2^2B_1 state, with its high intensity 0-0 band is natural, as shown in Figure 9. In addition to the 0-0 band, the prominent modes are 7, 10, 14, 16, 22, 29, 30, 33, 37 and 39.

Table VII. The 1^2A_1 state, calculated by the CAM-B3LYP method, as onset to the combined Bands D plus E. The highest intensity bands lie nearly 0.5 eV higher in energy and are shown in the supplementary material as SM6. 0-0 band 85967 cm^{-1}

| Energy / cm^{-1}	Excitation	Intensity	Energy / cm^{-1}	Excitation	Intensity
0	0	305	1394	$7^2;2^2$	89
320	5^1	370	1395	7^3	9583
465	7^1	1828	1406	$24^1;5^1$	130
640	5^2	242	1424	$7^1;5^3$	274
785	$7^1;5^1$	3071	1429	$18^1;7^1$	1059
866	15^1	37	1456	$26^1;5^1$	850
929	$7^1;2^2$	31	1502	34^1	40
930	7^2	5244	1506	$15^1;5^2$	54
960	5^3	54	1511	$7^2;3^2$	37
965	18^1	191	1552	$24^1;7^1$	384
1087	24^1	73	1569	$7^2;5^2$	3687
1105	$7^1;5^2$	1699	1576	$29^1;5^1$	206
1136	26^1	488	1601	$26^1;7^1$	2794
1186	$15^1;5^1$	75	1604	$18^1;5^2$	207
1249	$7^1;5^1;2^2$	52	1609	36^1	35
1250	$7^2;5^1$	7906	1639	$8^1;7^2;2^1$	27
1256	29^1	115	1645	$7^2;6^1;3^1$	40
1284	$18^1;5^1$	341	1651	$15^1;7^1;5^1$	398
1331	$15^1;7^1$	215	1659	$12^1;7^2$	32
1366	$7^1;5^1;3^2$	24	1680	$20^1;7^1;2^1$	31

Table VIII. Onset of the 2^2B_1 state, calculated by the CASSCF method. Energy of the 0-0 transition: 86290 cm^{-1}.

Energy / cm^{-1}	Excitation	Intensity	Energy / cm^{-1}	Excitation	Intensity
0	0	340500	811	$7^1;4^1;1^1$	1270
147	1^2	32620	814	$7^1;2^2;1^2$	393
256	2^2	8948	822	7^2	40900
294	1^4	4073	826	$10^1;1^2$	19080
349	$3^1;1^1$	2956	853	$8^1;5^1$	234
400	$4^1;1^1$	1539	853	$7^1;1^6$	451
403	$2^2;1^2$	855	875	14^1	19020
411	7^1	180900	892	$7^1;6^1;2^1$	5415
442	1^6	909	907	$7^1;3^1;1^3$	566
480	$6^1;2^1$	10330	909	$4^2;2^2$	290

496	$3^1;1^3$	693	912	16^1	122500
512	2^4	353	923	$7^1;2^4$	186
547	$4^1;1^3$	687	929	$12^1;2^1$	1908
550	3^2	2836	935	$10^1;2^2$	3658
558	$7^1;1^2$	15040	945	$9^1;3^1;1^2$	823
597	$9^1;1^1$	187	947	$4^2;1^4$	288
601	$4^1;3^1$	2662	958	$7^1;4^1;1^3$	318
627	$6^1;2^1;1^2$	977	961	$6^2;2^2$	383
643	$3^1;1^5$	255	961	$7^1;3^2$	2062
653	4^2	11080	970	$7^2;1^2$	5499
667	$7^1;2^2$	4741	973	$10^1;1^4$	2530
679	10^1	140000	1013	$7^1;4^1;3^1$	1330
697	$3^2;1^2$	631	1022	$14^1;1^2$	1581
706	$7^1;1^4$	3026	1027	$10^1;3^1;1^1$	1776
736	$6^1;2^3$	814	1039	$7^1;6^1;2^1;1^2$	444
760	$7^1;3^1;1^1$	1279	1053	$4^3;1^1$	234
798	$9^1;3^1$	5408	1059	$16^1;1^2$	17720
800	$4^2;1^2$	1067	1064	$7^1;4^2$	4773
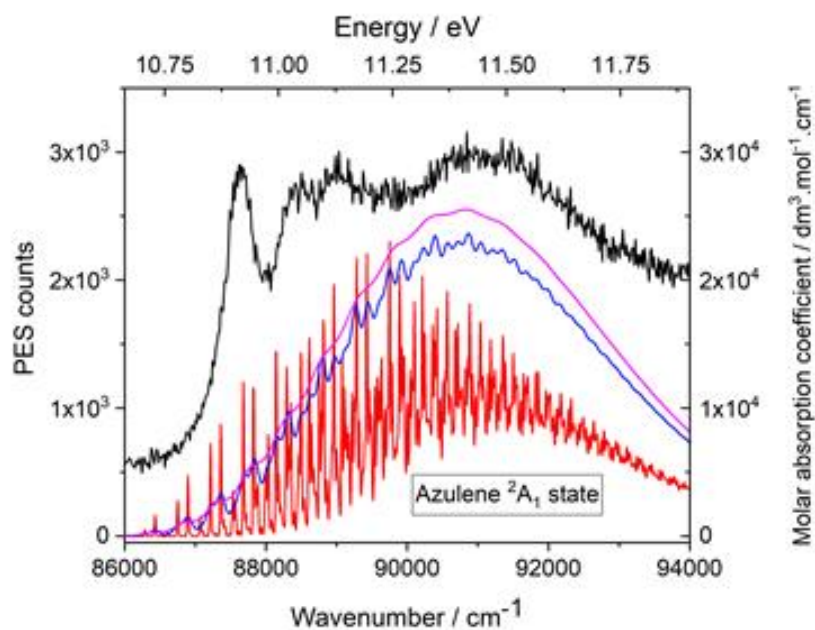
Figure 8. Bands D and E. An overlapping set of peaks assigned to the 2^2B_1 and 1^2A_1 ionic states determined using the CAM-B3LYP method. The theoretical levels of 1^2A_1 are overlaid and show sets of vibrational peaks corresponding to Half-Widths at Half-Maximum of 10 cm^{-1} (red), 70 cm^{-1} (magenta) and 150 cm^{-1} (blue).
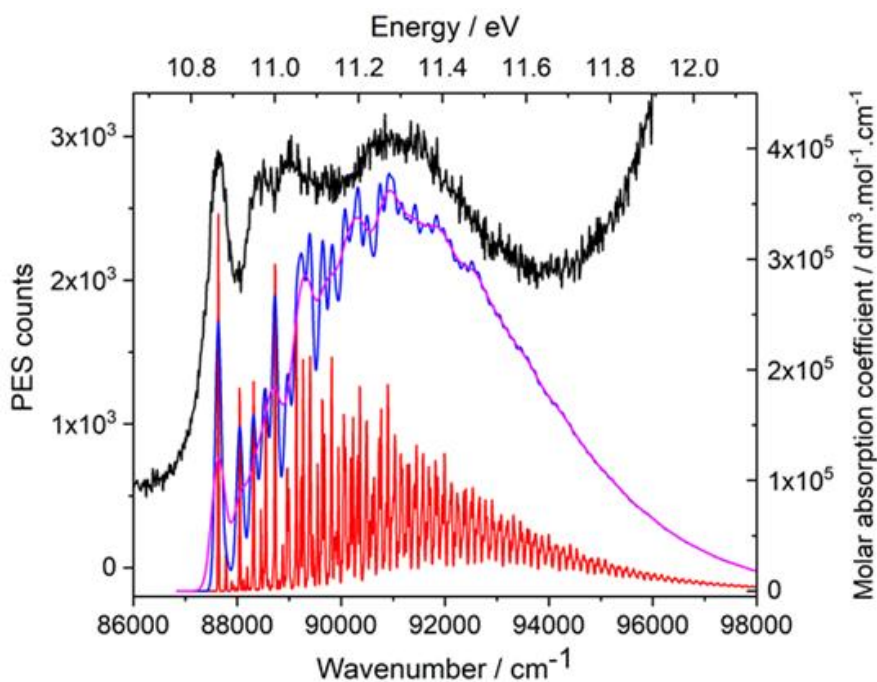
Figure 9. Bands D and E. The theoretical levels of the 2^2B_1 state, determined by the CASSCF method, is overlaid to show sets of vibrational peaks corresponding to Half-Widths at Half-Maximum of 10 cm^{-1} (red), 70 cm^{-1} (magenta) and 150 cm^{-1} (blue).

5. Comparison of the $^2A_2$ theoretical Franck-Condon envelope with the ZEKE spectrum.

We note that Tanaka et al[16] correlated fundamental vibrations for various electronically excited and ionic electronic states with neutral ground state vibrations in their ZEKE study. There is an implicit assumption that the sequence of frequencies exhibited are the same by symmetry. In the ZEKE study, the mass-selected ion-current spectrum obtained for neutral azulene, with the 0-0 band at 28758 cm^{-1}, is accompanied by vibrational peaks at higher frequencies: 239, 373, 468, 661, 746, 886 and 918 cm^{-1}. These frequencies are very similar to those in the previously observed fluorescence excitation spectrum of the S_2 singlet state by Fujii et al.[17] This resonance Raman study adopted the notation of Chao and Khanna,[44] who chose the mode sequence: a_1 (v_1 to v_{17}), a_2(v_{18} to v_{23}), b_1 (v_{24} to v_{39}), and b_2 (v_{40} to v_{48}), as noted above. This contrasts with the G-16 system, where b_1 has 9 modes, while b_2 has 16 modes. However, for simplicity, we have adopted, for this section only, to follow Tanaka et al.[16] to avoid complications. They attributed the ZEKE series of vibrations above,[16,43] to modes 39(b_1), 17(a_1), 38(b_1), 16(a_1), 17^2(a_1), 14^1(a_1) and 13^1(a_1) respectively. These are indicated in Figure 10, where the a_1 modes from the present study are shown in black, with the two b_1 vibrations of Tanaka

et al, shown in blue. Our calculated Franck-Condon vibrational frequencies for the 17, 16, 14 and 13 a_1 bands are in close agreement with their work. Further details of the procedure for re-generating the ZEKE spectrum are given in the supplementary material as SM7. Thus, we can interpolate the ZEKE spectrum with additional assignments as shown. Differences between the two studies have a maximum difference of 50 cm^{-1}, making these indistinguishable in Figure 10.

Two ZEKE vibrations were attributed to non-symmetric modes, which must occur via vibronic coupling with another state.[16,43] The fluorescence excitation spectral study, also led to the very small separation of v_{16} (a_1, 662 cm^{-1}) from v_{37} (b_1, 668 cm^{-1}). The observation of several b_1 vibrations in the ZEKE and other spectra probably comes from the vibronic coupling with the S_3 ($^1B_1$) state which lies 5000 cm^{-1} above the S_2 state. That is, the S_2 state borrows absorption intensity by coupling with both the S_4 ($^1A_1$) state and S_3($^1B_1$) states.[17]

Initially the theoretical 1^2A_2 Franck-Condon line intensities, using the CAM-B3LYP harmonic frequency results, were corrected for the difference in 0-0 band positions, and the results scaled between the two spectra. We correlated the 17^1, 16^1 and 14^1 bands, between the two sets of data, since our results are in agreement with Takana et al.[16] The correlation line is $v_{Calc}^{ZEKE} = 0.9714x \ v_{Calc}^{FC} + 1711$ cm^{-1}; thus, the whole theoretical spectrum has been shifted to higher energies by 1711 cm^{-1} (0.2121 eV); the energies are 97.1% of those measured experimentally. Overall, this is a very close correlation.

We performed a major expansion of the reported ZEKE spectrum,[16] as described in the supplementary material as SM7, to generate the much amplified blue line in Figure 10. Some variations in the band intensities may have occurred during this process, but intensities are not central to the theme.

In a second phase, we used the corresponding CAM-B3LYP anharmonic frequency determinations at the Franck-Condon level for the theoretical 1^2A_2 state. These results are shown in Figure 10 as a (red) stick diagram, superimposed on the (blue) ZEKE spectrum. Our data are shown in Table IX. An important conclusion is that the anharmonic calculations, using the same basis set and theoretical method for azulene, lead to a mean correction to fit the ZEKE data, that is reduced from 32.7 cm^{-1}

for the harmonic frequencies, to 11.1 cm^{-1} for the CAM-B3LYP anharmonic set. All the modes, marked in black in Figure 10, are Franck-Condon modes and hence of a$_1$ symmetry. The b$_1$ modes of Tanaka et al[16] are also labelled as 38 and 39 (in blue). The a$_1$ modes shown suggest that the ZEKE spectrum can be provisionally subject to further assignment of vibrational states in the ^{2}A$_2$ ionic state.
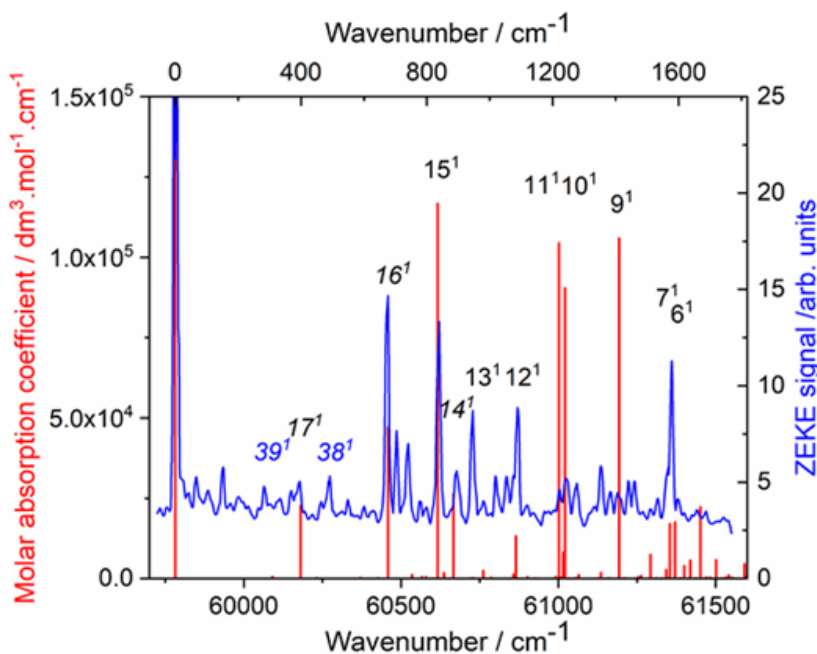
Figure 10. The ZEKE electron spectrum of azulene, from D. Tanaka, S. Sato, and K. Kimura, Chem. Phys. 239, 437–445 (1998), obtained via the S$_2$ origin (in blue). This is compared with the Franck-Condon profile for the 1^{2}A$_2$ state (in red), determined using the CAM-B3LYP method. Modes 39, 17, 38, 14 and 13, shown in italics are those proposed by Tanaka et al;[16] the a$_1$ group of these are consistent with the Franck-Condon analysis given here. Non-italicised modes are based on the present study.

Table IX. The non-scaled and scaled CAM-B3LYP anharmonic frequencies made to correlate with the ZEKE spectral frequencies.

Estimated peak positions in ZEKE spectrum. 0-0 band intensity is 100 units		Corrected[a] anharmonic calc. / cm^{-1}	Difference from ZEKE /cm^{-1}	Assignment G-16 ascending sequence	Standard a$_1$ assignment
Energy from 0-0 band / cm^{-1}	Relative local intensity /arbitrary units				
394	2	387	7.0	6^1	17^1
671	21	674	-3.4	10^1	16^1
835	12	836	-0.8	15^1	15^1
886	3	887	-0.6	17^1	14^1
938	10	951	-12.6	19^1	13^1
1079	7	1094	-14.8	26^1	12^1
1245	2	1229	16.2		11^1

1271	2	1252	18.8		10^1
1411	2	1418	-6.7		9^1
		1481	--		8^1
1580	6	1583	-3.2	39^1	7^1
		1593	--		6^1

Footnote to Table IX. (a) The anharmonic frequencies are directly related to the ZEKE set by: ν_{ZEKE} = 1.015*$\nu_{Anharmonic}$ - 25.314 cm^{-1}.

IV. Conclusions

Azulene is an historically important molecule, both experimentally and theoretically. In this paper, we reinvestigate its photoelectron spectrum with a view to interpretation of the vibrational structure disclosed by the present synchrotron based PES. The closely related ZEKE spectra fit closely into this study and are similarly analysed.

The two lowest ionization bands of the PES (bands A and B) both show a range of vibrations, which have been interpreted by Franck-Condon methods for the first time; superficially similar in appearance, there are significant differences in the principal modes present. The third ionization band C, is comparatively narrow in comparison to A and B; this is a result of only lower frequency vibrations occurring in band C. The onset of the combined band D+E has the appearance of a π-electron ionization, from its local high onset intensity and narrow width. The calculated sequence, however, shows that it is largely overlaid by the first σ-state, 1^2A_1. The greatly differing intensities of the 0-0 bands for these states enables a reasonable interpretation.

Above 11 eV, the PES shows a series of broad bands, each of which has the appearance of more than one ionisation lying underneath. Our single excitation CI study is in almost exact agreement with our symmetry adapted coupled cluster study, using the SAC-CI code, for this whole spectrum up to 19 eV. A number of shake-up states accompany the principal 1-electron ionizations, but rather fewer than previously suggested.[41]

The previously reported ZEKE spectrum,[16,43] is based upon the 1^2A_2 ionic state, under band A of the PES. We have found that the current triple-zeta with single polarization results both agree with most of the previous interpretation, but also offer an expansion of the number of modes present. The

separations of our theoretical a_1 symmetry fundamental modes for the 1^2A_2 state from the 0-0 band, match with those proposed by Tanaka et al[16] for modes 17, 16 and 14. This enables us to superimpose the most prominent a_1 fundamentals upon the ZEKE spectrum, and arrive at several new proposals for a_1 band positions. We are unable to offer an alternative explanation for any assignment based on non-symmetric vibrations, since our analysis was performed under Franck-Condon conditions. This is not to deny the possibility of such vibrations being present, but we propose that a simpler interpretation is possible for several more a_1 mode assignments.

SUPPLEMENTARY MATERIAL

See the supplementary material for additional information on each of the following:

Supplementary material as SM1. The multi-peak analysis. Supplementary material as SM2. The ground and ionic state structures. 3. Supplementary material as SM3. The MCSCF states. 4. Supplementary material as SM4. Tamm-Dancoff approximation (TDA). 5. Supplementary material as SM5. Full sequences of harmonic frequencies for ionic states of azulene. 6. Supplementary material SM6. Higher vibrational states from the 1^2A_1 Franck-Condon calculation. These higher combination bands are where the principal intensity lies and cover the region up to the band maximum. Supplementary material SM7. Recovery of the ZEKE spectrum shown in Figure 10.

ACKNOWLEDGEMENTS

DATA AVAILABILITY OF ARTICLE OR SUPPLEMENTARY MATERIAL.

The data that support the findings of this study, including its supplementary material, will be available from the corresponding author upon reasonable request.

REFERENCES

1. M. H. Palmer, M. Coreno, M. de Simone, C. Grazioli, S. V. Hoffmann, and N. C. Jones, J. Chem. Phys. 150, 194305 (2019). https://doi.org/10.1063/1.5096254

2. M. H. Palmer, S. V. Hoffmann, N. C. Jones, M. Coreno, M. de Simone, and C. Grazioli, J. Chem. Phys. 151, 084304 (2019). https://doi.org/10.1063/1.5115997

3. M. H. Palmer, R. A. Aitken, M. Coreno, M. de Simone, C. Grazioli, S. V. Hoffmann, and N. C. Jones, J. Chem. Phys. 152, 144301 (2020). https://doi.org/10.1063/1.5142268

4. M. H. Palmer, S. V. Hoffmann, N. C. Jones, M. Coreno, M. de Simone, C. Grazioli, and R. A. Aitken, J. Chem. Phys. 153, 054301 (2020). https://doi.org/10.1063/5.0011088

5. M. H. Palmer, M. Coreno, M. de Simone, C. Grazioli, R. A. Aitken, S. V. Hoffmann, N. C. Jones, and C. Peureux, J. Chem. Phys. 153, 204303 (2020).https://doi.org/10.1063/5.0031387

6. M. H. Palmer, S. V. Hoffmann, N. C. Jones, M. Coreno, M. de Simone, C. Grazioli, and R. A. Aitken, J. Chem. Phys. 155, 034308 (2021). https://doi.org/10.1063/5.0053962

7. H. H. Jaffe and M. Orchin, 'Theory and Applications of Ultraviolet Spectroscopy', Chapter 13.9, p337–344, Wiley, New York (1962).

8. R. G. Parr, 'The Quantum Theory of Molecular Electronic Structure, Benjamin, New York, p58 (1964).

9. G. M. Badger, 'Aromatic Character and Aromaticity', Cambridge University Press; (ISBN: 9780521095433); Cambridge Texts in Chemistry and Biochemistry, (1969).

10. L.Salem, 'The Molecular Orbital Theory of Conjugated systems', Chapters 1-5 and 1-6, W. A. Benjamin, New York, (1966).

11. J. H. D. Eland and C. J. Danby, Z. Naturforsch. A 23, 355–357 (1968). https://doi.org/10.1515/zna-1968-0304

12. R. Boschi, E. Clar, and W. Schmidt, J. Chem. Phys. 60, 4406–4418 (1974). https://doi.org/10.1063/1.1680919

13. P. M. Weber and N. Thantu, Chem. Phys. Lett. 197, 556–561, (1992). https://doi.org/10.1016/0009-2614(92)85815-R

14. H. J. Tobler, A. Bauder, and Hs. H.Günthard, J. Mol. Spectrosc. 18, 239–246 (1965). https://doi.org/10.1016/0022-2852(65)90139-6

15. (a) S. Huber, G. Grassi, and A. Bauder, Mol. Phys. 103, 1395–1409 (2005). https://doi.org/10.1080/00268970500038451; (b) S. Thorwirth, P. Theulé, C. A. Gottlieb, M. C. McCarthy, and P. Thaddeus, Astrophys. J. 662, 1309–1314 (2007). https://doi.org/10.1086/518026

16. D. Tanaka, S. Sato, and K. Kimura, Chem. Phys. 239, 437–445 (1998). https://doi.org/10.1016/S0301-0104(98)00312-7

17. M. Fujii, T. Ebata, N. Mikami, and M. Ito, Chem. Phys. 77, 191–200 (1983). https://doi.org/10.1016/0301-0104(83)85076-9

18. R. S. Chao and R. K. Khanna, Spectrochim. Acta, Part A, 33, 53–62 (1977). https://doi.org/10.1016/0584-8539(77)80147-5

19. V. Barone, J. Bloino, M. Biczysko, and F. Santoro, J. Chem. Theory Comput. 5, 540–554 (2009). https://doi.org/10.1021/ct8004744

20. J. Bloino, M. Biczysko, F. Santoro, and V. Barone, J. Chem. Theory Comput. 6, 1256–1274 (2010). https://doi.org/10.1021/ct9006772

21. A. Baiardi, J. Bloino, and V. Barone, J. Chem. Theory Comput. 9, 4097–4115 (2013). https://doi.org/10.1021/ct400450k

22. M. J. Frisch, G. W. Trucks, H. B. Schlegel, G. E. Scuseria, M. A. Robb, J. R.Cheeseman, G. Scalmani, V. Barone, G. A. Petersson, H. Nakatsuji, X. Li, M.Caricato, A. V. Marenich, J. Bloino, B. G. Janesko, R. Gomperts, B. Mennucci,H. P. Hratchian, J. V. Ortiz, A. F. Izmaylov, J. L. Sonnenberg, D. Williams-Young,F. Ding, F. Lipparini, F. Egidi, J. Goings, B. Peng, A. Petrone, T. Henderson, D.Ranasinghe, V. G. Zakrzewski, J. Gao, N. Rega, G. Zheng, W. Liang, M. Hada,M. Ehara, K. Toyota, R. Fukuda, J. Hasegawa, M. Ishida, T. Nakajima, Y. Honda,O. Kitao, H. Nakai, T. Vreven, K. Throssell, J. A. Montgomery, Jr., J. E.Peralta, F.Ogliaro, M. J. Bearpark, J. J. Heyd, E. N. Brothers, K. N. Kudin, V. N. Staroverov, T.A. Keith, R. Kobayashi, J. Normand, K. Raghavachari, A. P. Rendell, J. C. Burant,S. S. Iyengar, J. Tomasi, M. Cossi, J. M. Millam, M. Klene, C. Adamo, R. Cammi,J. W. Ochterski, R. L. Martin, K. Morokuma, O. Farkas, J. B. Foresman, and D. J. Fox, Gaussian 16, Revision A.03, Gaussian, Inc.,Wallingford, CT, 2016.

23. R. G. Parr and W. Yang, Density-Functional Theory of Atoms and Molecules, Oxford University Press, Oxford, 1989.

24. A. D. Becke, J. Chem. Phys. 98, 5648–5652 (1993). https://doi.org/10.1063/1.464913

25. T. Yanai, D. P. Tew, and N. C. Handy, Chem. Phys. Lett. 393, 51–57 (2004). https://doi.org/10.1016/j.cplett.2004.06.011

26. S. Grimme, J. Chem. Phys. 124, 034108 (2006). https://doi.org/10.1063/1.2148954

27. S. Grimme, S. Ehrlich, and L. Goerigk, J. Comp. Chem. 32 1456–1465 (2011). https://doi.org/10.1002/jcc.21759

28. T. Schwabe and S. Grimme, Phys. Chem. Chem. Phys. 9 3397–3406 (2007). https://doi.org/10.1039/B704725H

29. H.-J. Werner P. J. Knowles F. R. Manby M. Schütz P. Celani T. Korona R. Lindh A. Mitrushenkov G. Rauhut K. R. Shamasundar T. B. Adler R. D. Amos A. Bernhardsson A. Berning D. L. Cooper M. J. O. Deegan A. J. Dobbyn F. Eckert E. Goll C. Hampel A. Hesselmann G. Hetzer T. Hrenar G. Jansen C. Köppl Y. Liu A. W. Lloyd R. A. Mata A. J. May S. J. McNicholas W. Meyer M. E. Mura A. Nicklaß D. P. O'Neill P. Palmieri K. Pflüger R. Pitzer M. Reiher T. Shiozaki H. Stoll A. J. Stone R. Tarroni T. Thorsteinsson M. Wang and A. Wolf MOLPRO Version 2012.1 a package of ab initio programs 2012 see http://www.molpro.net.

30. R. Ahlrichs and P. R. Taylor, J. Chim. Phys. 78, 315–324 (1981). https://doi.org/10.1051/jcp/1981780315

31. A. Schaefer, H. Horn, and R. Ahlrichs, J. Chem. Phys. 97, 2571–2577 (1992). https:doi/org/10.1063/1.463096

32. H. Nakatsuji and K. Hirao, Int. J. Quantum Chem. 20, 1301–1313 (1981). https://doi.org/10.1002/qua.560200613

33. H. Nakatsuji and T. Yonezawa, Chem. Phys. Lett. 87, 426–431 (1982). https://doi.org/10.1016/0009-2614(82)83004-2

34. H. Nakatsuji, Chem. Phys. 75, 425–411 (1983). https://doi.org/10.1016/0301-0104(83)85209-4

35. H. Nakatsuji, Int. J. Quantum Chem. Symp. 24 (S17), 241–255 (1983). https://doi.org/10.1002/qua.560240830

36. H. Nakatsuji, K. Ohta, and T. Yonezawa, J. Phys. Chem. 87, 3068–3074 (1983). https://doi.org/10.1021/j100239a022

37. W. von Niessen, L. S. Cederbaum, and W. P. Kraemer, J. Chem. Phys. 65, 1378–1386 (1976). https://doi.org/10.1063/1.433244

38. L. S. Cederbaum and W . Domcke, Advance in Chemical Physics, Volume XXXVI, p.205-344, Edited by I. Prigogine, Stuart A. Rice, Wiley and Sons, Inc.

39. W. von Neissen, J. Schirmer, and L. S. Cederbaum, Comp. Phys. Rep., 1, 57–125 (1984). https://doi.org/10.1016/0167-7977(84)90002-9

40. M. F. Guest, I. J. Bush, H. J. J. Van Dam, P. Sherwood, J. M. H. Thomas, J. H.Van Lenthe, R. W. A. Havenith, and J. Kendrick, Mol. Phys. 103, 719–747 (2005). https://doi.org/10.1080/00268970512331340592

41. M. S. Deleuze, J. Chem. Phys, 116, 7012–7026 (2002). https://doi.org/10.1063/1.1462615

42. R. J. Buenker and S. G. Peyerimhoff, Chem. Phys. Lett. 3, 37–42 (1969). https://doi.org/10.1016/0009-2614(69)80014-X

43. K. Kimura, J. Electron Spectrosc. and Related Phenomena, 100, 273–296 (1999). https://doi.org/10.1016/S0368-2048(99)00051-1

44. R. S. Chao and R. K. Khanna, Spectrochim. Acta, Part A 33, 53–62 (1977). https://doi.org/10.1016/0584-8539(77)80147-5